AIP Applied Physics Letters

Towards the development of a virtual organic solar cell: An experimental and dynamic Monte Carlo study of the role of charge blocking layers and active layer thickness

K. Feron, C. J. Fell, L. J. Rozanski, B. B. Gong, N. Nicolaidis, W. J. Belcher, X. Zhou, E. Sesa, B. V. King, and P. C. Dastoor

Citation: Applied Physics Letters **101**, 193306 (2012); doi: 10.1063/1.4767291
View online: http://dx.doi.org/10.1063/1.4767291
View Table of Contents: http://scitation.aip.org/content/aip/journal/apl/101/19?ver=pdfcov
Published by the AIP Publishing

Towards the development of a virtual organic solar cell: An experimental and dynamic Monte Carlo study of the role of charge blocking layers and active layer thickness

K. Feron,[1,2,a)] C. J. Fell,[1,2] L. J. Rozanski,[1] B. B. Gong,[3] N. Nicolaidis,[2] W. J. Belcher,[2] X. Zhou,[2] E. Sesa,[2] B. V. King,[2] and P. C. Dastoor[2]
[1]*CSIRO Energy Technology, Newcastle, NSW 2300, Australia*
[2]*University of Newcastle, Centre for Organic Electronics, Newcastle, NSW 2308, Australia*
[3]*University of New South Wales, Mark Wainwright Analytical Centre, Sydney, NSW 2052, Australia*

(Received 30 July 2012; accepted 29 October 2012; published online 8 November 2012)

Monte Carlo (MC) simulations have been used to fully model organic solar cells. The quantum efficiency and short-circuit current of these virtual devices are in excellent agreement with experimental measurements. Simulations show that, contrary to expectation, indium tin oxide/poly(3,4-ethylenedioxythiophene) poly(styrenesulfonate)/poly(3-hexylthiophene):[6,6]-phenyl-C61-butyric acid methylester (PCBM)/aluminium devices lack effective charge blocking layers at the electrode interfaces. X-ray photoelectron spectroscopy depth profiling shows that despite a PCBM-rich region near the cathode, interface intermixing at the electrodes combined with incomplete PCBM coverage leads to significant interface recombination. This work highlights the effectiveness of MC simulations as a predictive tool and emphasizes the need to control electrode interface processes. © *2012 American Institute of Physics*. [http://dx.doi.org/10.1063/1.4767291]

Dynamic Monte Carlo (MC) simulations are a well-established approach to modelling organic photovoltaic (OPV) devices.[1–6] The MC approach allows for a full treatment of the relevant processes in an organic solar cell (including light absorption and subsequent transport, dissociation and recombination of excitons, and free charges) while accounting for the blend morphology of the photoactive layer.[7–9] In principle, the MC approach allows for the development of a "virtual solar cell" whereby, for a known morphology, OPV performance could be predicted by modelling these internal processes. However, although MC simulations have been shown to describe experimental observations qualitatively,[2,3,5,10] a direct quantitative comparison of modelled and experimentally measured OPV performance indicators such as internal quantum efficiency (IQE) and short-circuit current density (J_{sc}) for a specific OPV system is still lacking. Here, we report a quantitative description of bulk heterojunction (BHJ) OPV devices with the conventional structure indium tin oxide (ITO)/poly(3,4-ethylenedioxythiophene) poly(styrenesulfonate) (PEDOT:PSS)/poly(3-hexylthiophene) (P3HT): [6,6]-phenyl-C61-butyric acid methylester (PCBM)/aluminium (Al) using a dynamic Monte Carlo approach.

A first-reaction method, which has been shown to model charge dynamics accurately for materials such as P3HT and PCBM,[11] is applied to decrease the computational burden. The internal optical field, and thus the exciton generation profile, in our devices has been determined using transfer matrix techniques as described previously,[12,13] using optical models similar to those used by others[14,15] and used in previous work.[16] Exciton transport is modelled according to Förster resonance energy transfer theory.[17,18] The hopping behaviour of charges that are created at the P3HT:PCBM heterointerface after exciton dissociation is modelled using Marcus theory.[17,19] The coulomb interaction between charges and image charges (surface charge induced at electrodes) is taken into account. The sphere of electrostatic influence of each charge carrier is taken as the ceiling of the thermal capture radius. The reorganisation energy, λ, was chosen to be 0.5 eV, which is in the range of commonly accepted values used in these simulations[1,17] and is in accordance with experimental data.[20] Charge extraction is described using Marcus theory.[2,3] Conventional values for the energy levels and other relevant parameters were used (Table I). Morphologies with a feature size (defined as 3 V/A, where V is volume and A is interfacial area of the two organic moieties) of 14.2 nm were generated using a cellular automata method.[17,21] The BHJ morphologies did not contain isolated islands and formed an interpenetrating network from one electrode to the other (see supplementary material for a depiction of the morphologies[44]). The feature size used here is comparable to domain sizes used in other Monte Carlo models[2,4,5] and is in accordance with an estimation of P3HT:PCBM domain sizes based on atomic force microscopy phase imaging.[22] At this feature size exciton dissociation is efficient (~95%), which correlates with the almost complete quenching of photoluminescence observed in these devices.[23–25] Approximately, 50% of the anode was covered by P3HT and 50% of the cathode was covered by PCBM unless blocking layers were simulated, in which case the blocking layer ensures 100% electrode coverage by the desired material.

OPV devices were fabricated on glass substrates with patterned ITO after cleaning with a series of solvent sonications and a 15 min plasma treatment in a mixture of air and pure oxygen. A 40 nm layer of PEDOT:PSS was applied by spincasting, then annealed for 10 min at 140 °C. The annealing was conducted in an inert environment, as were all

a)Author to whom correspondence should be addressed. Electronic mail: Krishna.Feron@csiro.au.

TABLE I. Parameters used in the Monte Carlo simulations.

Property	Value	Reference
Temperature (T)	300 K	
Relative dielectric constant	3.1	Ref. 26
Standard deviation density of states P3HT and PCBM	0.05 eV	As determined from absorption spectra
Forster radius PCBM	3.65 nm (equivalent to 1D diffusion length of 40 nm)	Ref. 21 (PCBM diffusion length is assumed to be the same as C_{60})
Forster radius P3HT	2.15 nm (equivalent to 1D diffusion length of 8.5 nm)	Ref. 27
Exciton lifetime PCBM	11 μs	Ref. 28
Exciton lifetime P3HT	400 ps	Ref. 27
Charge mobility PCBM	1×10^{-7} m^2/V/s	Ref. 29
Charge mobility P3HT	3–3.34 $\times 10^{-6}$ m^2/V/s	Ref. 30
Charge carrier recombination rate	1×10^4 s^{-1}	
Reorganization energy (λ)	0.5 eV	
Lattice constant	1 nm	Ref. 17
PEDOT:PSS energy level	−5.1 eV	Ref. 31
Aluminium work function	−4.3 eV	Ref. 31
P3HT HOMO	−5.1 eV	Ref. 31
PCBM LUMO	−4.3 eV	Ref. 31

subsequent fabrication steps. A 1:1 blend of P3HT and PCBM was dissolved in chlorobenzene with various concentrations to obtain various thicknesses. The solution was filtered (0.2 μm), and then spincast on top of the annealed PEDOT:PSS to form the active layer of the device. A 100 nm thick Al cathode layer was deposited by evaporation. The samples were then annealed for 4 min at 140 °C. Short circuit current density was obtained from the device current-voltage (I-V) curves measured under AM1.5 illumination (light source is a Newport Oriel class A model 91160 A solar simulator) using a Keithley SourceMeter (model 2400). These measurements were converted into total IQE by modelling the true absorption of the photoactive materials to determine the total number of absorbed photons and by calculating the total number of extracted electrons from the J_{sc} measurements. Since the devices were small (<1 cm^2), the real J_{sc} in the absence of edge-effects was established by measuring devices of different sizes and extrapolating to large area (see supplementary material[44]). 12 different devices were fabricated at each thickness and the average IQE and J_{sc} values together with the corresponding standard deviations were calculated.

As shown in Figs. 1(a) and 1(b), there is excellent agreement between the experimental and modelled results, with the data generated for the virtual organic solar cell corresponding to the measured values to within the statistical error of the measurements.

For an optimal device, holes are transported to the ITO anode and electrons to the metal cathode exclusively and subsequently extracted into the external circuit. However, in the absence of a selective electrode or a blocking layer, it is possible for charge carriers to hop into the opposite polarity electrode (albeit with a smaller probability) resulting in reduced device efficiency. For the P3HT:PCBM system, it is well known that thermal annealing affects the vertical composition of the active layer,[32] leading to enrichment of the components at the electrode interfaces.[33] Indeed, previous work has indicated that annealed P3HT:PCBM devices

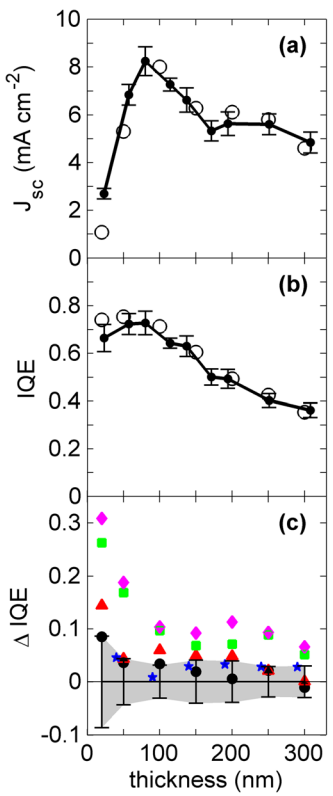

FIG. 1. J_{sc} (a) and IQE (b) as a function of thickness. Dots are measured results and open circles are modelled data. A line is drawn through the experimental results as a guide to the eye. Discrepancy between modelled data and measured IQE data (c) is shown as a function of thickness for the four virtual device structures initially modelled: (i) Black dots correspond to a device without blocking layers, (ii) red triangles to a device where a perfect blocking layer is used at the cathode (i.e., PCBM capping layer) only, (iii) green squares to a device where a perfect blocking layer is used at the anode (i.e., PEDOT:PSS) only and (iv) magenta diamonds to a device where two blocking layers are used. Also shown (blue pentagrams) is the discrepancy between modelled data and measured IQE data for the actual annealed device structure with partial P3HT (58% anode coverage) and PCBM (60% cathode coverage) blocking layers as subsequently determined by x-ray photoelectron spectroscopy measurements. Error bars and shading indicate the statistical error (standard deviation) of the measured values.

should contain P3HT-rich and PCBM-rich blocking layers at the anode and cathode, respectively, resulting in improved electrode selectivity.[32]

In order to establish the theoretical effectiveness of these blocking layers, we initially modelled 4 different solar cell configurations: (1) blocking layers at both electrodes, (2) one blocking layer at the anode, (3) one blocking layer at the cathode, and (4) no blocking layers. Fig. 1(c) shows the difference between the modelled and experimental IQE values (ΔIQE) for each of the initial 4 configurations, with the error bars and shaded region showing the standard deviation in the experimental measurement. It is clear that ΔIQE is minimised for the model with no blocking layers and that, surprisingly, the addition of blocking layers at the electrodes results in a progressively poorer fit to the data. As such, the MC model suggests that, contrary to expectation, there are no effective blocking layers present in this experimental system.

In order to gain further insight into the dominant recombination mechanisms that are operating for each model, we have calculated separately the total bulk recombination efficiency (which consists of bimolecular, geminate and exciton recombination)[34] and the interface recombination efficiency. Fig. 2 shows the bulk and interface recombination efficiency as a function of thickness for each model and reveals that, in the absence of any blocking layers, interface recombination is significant for all thicknesses and increases for thinner films. The optimal device efficiency is obtained for an active layer thickness of ~80 nm, which correlates well with the intersection point of the bulk and interface recombination efficiencies. Interestingly, although interface recombination efficiency is lowered in the presence of a cathode blocking layer, the reduction is moderate. On the other hand, an anode blocking layer leads to a large increase in performance. This difference in performance gain is related to the difference in the number of excitons generated near the cathode and anode. When the system contains blocking layers at both electrodes, interface recombination is necessarily eliminated for all thicknesses. In order to quantify the relative importance of the two mechanisms, the ratio of interface to bulk recombination (for the model of best fit) is plotted in Fig. 2(e). As might be expected, for thin layers (<100 nm), recombination is substantially influenced by the electrode interfaces, but for thicker layers interface recombination has a minimal impact on device performance.

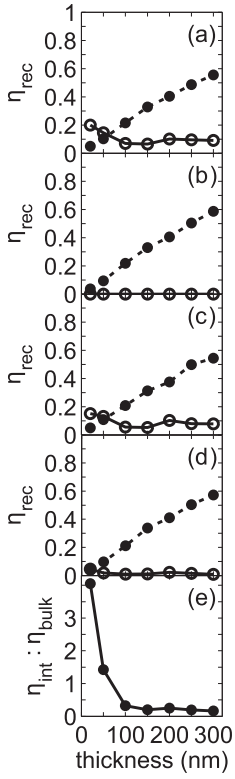

FIG. 2. Interface recombination efficiency (open circles) and bulk recombination efficiency (filled circles) as a function of thickness for a virtual device with (a) no blocking layers, (b) blocking layers at both electrodes, (c) only one blocking layer at the cathode, and (d) only one blocking layer at the anode. (e) shows the ratio between interface recombination and bulk recombination and indicates to what degree interface recombination dominates.

In order to determine directly the vertical composition of the P3HT:PCBM devices, x-ray photoelectron spectroscopy (XPS) depth profiling measurements using an argon sputtering source were conducted on annealed and unannealed devices (Fig. 3). The composition as a function of depth was tracked by measuring the change in the area of the elemental XPS peak relevant to the component of interest. Thus, the aluminium layer is directly identified by measuring the Al 2p peak, the active layer is identified from the carbon 1s peak and the anode is tracked by looking at the indium $3d_{5/2}$ peak. In addition, by monitoring the sulphur 2p signal and the carbon:sulphur (C:S) ratio, it is possible to monitor both the relative P3HT:PCBM concentration and to differentiate between the active and PEDOT:PSS layers.[35,36]

Figs. 3(a) and 3(b) show the XPS depth profiles for the unannealed and annealed devices, respectively. Whereas the unannealed device exhibits a constant PCBM:P3HT ratio throughout the active layer, it is clear that in the annealed device the carbon concentration is higher at the cathode than in the middle of the active layer suggesting that PCBM has segregated to the top electrode. In fact, we calculate that the PCBM concentration is 1.5 times higher near the cathode than in the bulk of the layer. In both cases, the C:S ratio is constant in the middle of the active layer and then decreases to a lower plateau before reaching the substrate interface; consistent with the presence of a P3HT:PCBM layer atop a PEDOT:PSS layer. Thus, the XPS data supports the prediction that, upon annealing, PCBM migrates to the cathode. In principle, therefore, the presence of a PCBM-rich region at the top electrode, coupled with a PEDOT:PSS layer at the substrate interface, should result in blocking layers at both interfaces; contrary to the conclusions of the MC modelling shown in Fig. 1.

However, there are a number of possible explanations for the apparent inconsistency between the observation of interface layers in the device and the fact that the best fit MC model contained no blocking layers. First, interdiffusion is known to occur between the metal electrode and the blocking layer resulting in an incomplete blocking layer.[37] The broad cathode and anode interface widths shown in Fig. 3 arise from interdiffusion during device fabrication and from ion beam mixing effects induced by the incident 3 kV Ar ion beam.[38] The widths of the Al/P3HT:PCBM (cathode) and PEDOT:PSS/ITO (anode) interfaces were measured to be

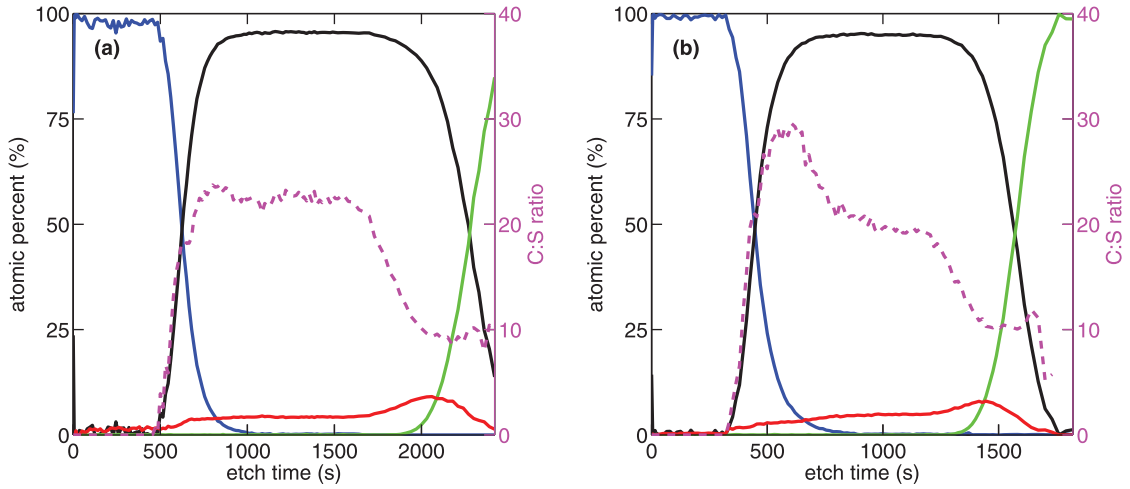

FIG. 3. XPS depth profiling results for: (a) an unannealed OPV device (active layer thickness of 60 nm) and (b) an annealed OPV device (active layer thickness of 80 nm). Blue indicates Al 2p (i.e., aluminium cathode), black C 1s (i.e., active layer and PEDOT:PSS layer), red S 2p (i.e., active layer and PEDOT:PSS layer), green In $3d_{5/2}$ (i.e., ITO anode) and magenta indicates the C 1s: S 2p ratio. The unannealed device (a) has a constant PCBM:P3HT ratio throughout the active layer, whereas the annealed device (b) has more PCBM at the cathode interface.

11.1 nm and 14.4 nm, respectively (see supplementary material). These widths are marginally larger than the interface width due to ion beam mixing (10.7 nm), which we have calculated to a first approximation using the TRIDYN-FZR simulation package[39] (see supplementary material). As such, the depth profiling measurements indicate that interpenetration of aluminium into the PCBM rich layer and indium into the PEDOT:PSS layer occurs within 10–20 nm of the interface, consistent with previous reports.[37] Second, the measured PCBM enrichment (1.5 times the P3HT concentration by weight) at the cathode would only lead to a 60% PCBM coverage and hence result in an incomplete PCBM interface layer. Finally, PEDOT:PSS has actually been shown to have relatively poor electron-blocking properties.[40,41] This combination of: (a) interdiffusion at the electrodes, (b) incomplete PCBM layer formation at the cathode, and (c) poor PEDOT:PSS electron-blocking capability at the anode would eliminate any blocking effect of these interface layers; consistent with the significant interface recombination and poor electron/hole blocking properties that are predicted by the Monte Carlo simulations and explaining why the best fit is obtained when assuming no blocking layers at all. In order to test this hypothesis, a fifth set of simulations were run using the electrode coverage indicated by the XPS measurements, i.e., 58% of the anode is in contact with P3HT and 60% of the cathode is in contact with PCBM. As shown in Fig. 1(c), the performance of this fifth virtual device structure agrees with the experimental data to within the statistical error of the measurements, thus demonstrating that the device performance as a function of active layer thickness is consistent with the absence of effective blocking layers.

Thus, a consistent picture has emerged, with the simulation indicating that there are no perfect blocking layers present, in agreement with the observed intermixing at the electrode interfaces. The excellent agreement between the modelled and experimental photocurrent data, supported by the conclusions from the XPS analysis provides confidence that the simulation is indeed accurately representing real device performance. Returning then to the simulation results, we see that the model predicts that OPV devices with blocking layers are actually more efficient for all thicknesses (Fig. 1) and that interface recombination is the dominant loss mechanism (Fig. 2). Possible interfacial recombination mechanisms include reverse diffusive recombination at contacts[34,42] or recombination through defects or impurity states at the interface for thin devices.[43] As such, the simulation suggests that improving the selectivity of the electrodes will lead to an increase in device performance.

In conclusion, we have shown that dynamic Monte Carlo models are not only useful from a qualitative point of view, but also correspond well with experimental data from a quantitative perspective. We have quantified the effect of interface recombination on device performance as a function of thickness and have shown that electrode interfaces dominate the performance of P3HT:PCBM devices for thin active layers (<100 nm) and remains significant until a thickness of ~150 nm. Furthermore, XPS depth profiling reveals the presence of substantial interface mixing at both electrodes. This observation, combined with the fact that the PCBM rich region at the cathode interface cannot provide complete coverage and that PEDOT:PSS has poor electron blocking properties, leads to the significant interface recombination that is predicted by the Monte Carlo simulations. Modelling suggests that a substantial performance gain may be achieved by improving charge selectivity at the anode, while charge selectivity improvements at the cathode result in a smaller performance increase. Overall, this work highlights the effectiveness of Monte Carlo simulations as a predictive tool and, in doing so, emphasizes the need to understand and control interface processes in OPV devices.

[1]C. Groves, J. C. Blakesley, and N. C. Greenham, Nano Lett. **10**, 1063 (2010).
[2]R. A. Marsh, C. Groves, and N. C. Greenham, J. Appl. Phys. **101**, 083509 (2007).
[3]L. Meng, D. Wang, Q. Li, Y. Yi, J.-L. Brédas, and Z. Shuai, J. Chem. Phys. **134**, 124102 (2011).
[4]P. K. Watkins, A. B. Walker, and G. L. B. Verschoor, Nano Lett. **5**, 1814 (2005).

[5]F. Yang and S. R. Forrest, ACS Nano **2**, 1022 (2008).
[6]R. G. E. Kimber, A. B. Walker, G. E. Schröder-Turk, and D. J. Cleaver, Phys. Chem. Chem. Phys. **12**, 844 (2010).
[7]T. M. Clarke and J. R. Durrant, Chem. Rev. **110**, 6736 (2010).
[8]P. W. M. Blom, V. D. Mihailetchi, L. J. A. Koster, and D. E. Markov, Adv. Mater. **19**, 1551 (2007).
[9]G. Li, R. Zhu, and Y. Yang, Nat. Photonics **6**, 153 (2012).
[10]V. I. Arkhipov, E. V. Emelianova, Y. H. Tak, and H. Bässler, J. Appl. Phys. **84**, 848 (1998).
[11]C. Groves, R. G. E. Kimber, and A. B. Walker, J. Chem. Phys. **133**, 144110 (2010).
[12]H. Hoppe, M. Niggemann, C. Winder, J. Kraut, R. Hiesgen, A. Hinsch, D. Meissner, and N. S. Sariciftci, Adv. Funct. Mater. **14**, 1005 (2004).
[13]L. A. A. Pettersson, L. S. Roman, and O. Inganäs, J. Appl. Phys. **86**, 487 (1999).
[14]H. Hoppe, N. S. Sariciftci, and D. Meissner, Mol. Cryst. Liq. Cryst. **385**, 113 (2002).
[15]M. C. Gurau, D. M. Delongchamp, B. M. Vogel, E. K. Lin, D. A. Fischer, S. Sambasivan, and L. J. Richter, Langmuir **23**, 834 (2007).
[16]N. C. Nicolaidis, B. S. Routley, J. L. Holdsworth, W. J. Belcher, X. Zhou, and P. C. Dastoor, J. Phys. Chem. C **115**, 7801 (2011).
[17]K. Feron, X. Zhou, W. J. Belcher, and P. C. Dastoor, J. Appl. Phys. **111**, 044510 (2012).
[18]T. Förster, Ann. Phys. **437**, 55 (1948).
[19]R. Marcus, Rev. Mod. Phys. **65**, 599 (1993).
[20]H. Imahori, K. Tamaki, D. M. Guldi, C. Luo, M. Fujitsuka, O. Ito, Y. Sakata, and S. Fukuzumi, J. Am. Chem. Soc. **123**, 2607 (2001).
[21]P. Peumans, A. Yakimov, and S. R. Forrest, J. Appl. Phys. **93**, 3693 (2003).
[22]S. Falke, P. Eravuchira, A. Materny, and C. Lienau, J. Raman Spectrosc. **42**, 1897 (2011).
[23]Y. Kim, S. A. Choulis, J. Nelson, D. D. C. Bradley, S. Cook, and J. R. Durrant, J. Mater. Sci. **40**, 1371 (2005).
[24]J. Liu, K.-L. Choy, and X. Hou, J. Mater. Chem. **21**, 1966 (2011).
[25]N. A. Nismy, K. D. G. I. Jayawardena, A. A. D. T. Adikaari, and S. R. P. Silva, Adv. Mater. **23**, 3796 (2011).
[26]P. Yu, D. Mencaraglia, A. Darga, A. Migan, R. Rabdbeh, B. Ratier, and A. Moliton, Phys. Status Solidi C **7**, 1000 (2010).
[27]P. E. Shaw, A. Ruseckas, and I. D. W. Samuel, Adv. Mater. **20**, 3516 (2008).
[28]S. Cook, H. Ohkita, J. R. Durrant, Y. Kim, J. J. Benson-Smith, J. Nelson, and D. D. C. Bradley, Appl. Phys. Lett. **89**, 101128 (2006).
[29]E. von Hauff, V. Dyakonov, and J. Parisi, Sol. Energy Mater. Sol. Cells **87**, 149 (2005).
[30]A. Mozer, N. Sariciftci, A. Pivrikas, R. Österbacka, G. Juška, L. Brassat, and H. Bässler, Phys. Rev. B **71**, 1 (2005).
[31]Y. S. Eo, H. W. Rhee, B. D. Chin, and J.-W. Yu, Synth. Met. **159**, 1910 (2009).
[32]M. Campoy-Quiles, T. Ferenczi, T. Agostinelli, P. G. Etchegoin, Y. Kim, T. D. Anthopoulos, P. N. Stavrinou, D. D. C. Bradley, and J. Nelson, Nature Mater. **7**, 158 (2008).
[33]A. J. Parnell, A. D. F. Dunbar, A. J. Pearson, P. A. Staniec, A. J. C. Dennison, H. Hamamatsu, M. W. A. Skoda, D. G. Lidzey, and R. A. L. Jones, Adv. Mater. **22**, 2444 (2010).
[34]R. A. Street and M. Schoendorf, Phys. Rev. B **81**, 1 (2010).
[35]Z. Xu, L. M. Chen, G. Yang, C. H. Huang, J. Hou, Y. Wu, G. Li, C. S. Hsu, and Y. Yang, Adv. Funct. Mater. **19**, 1227 (2009).
[36]S.-Y. Ma, Y.-M. Shen, P.-C. Yang, C.-S. Chen, and C.-F. Lin, Org. Electron. **13**, 297 (2012).
[37]H. J. Kim, H. H. Lee, and J.-J. Kim, Macromol. Rapid Commun. **30**, 1269 (2009).
[38]D. Briggs and M. P. Seah, *Practical Surface Analysis: Ion and Neutral Spectroscopy (Volume 2)* (Wiley, Chichester, 1996).
[39]W. Möller and M. Posselt, *TRIDYN-FZR User Manual, FZR-317* (Institute of Ion Beam Physics and Materials Research, Forschungzentrum Rossendorf, 2001).
[40]H. Yan, P. Lee, N. R. Armstrong, A. Graham, G. A Evmenenko, P. Dutta, and T. J. Marks, J. Am. Chem. Soc. **127**, 3172 (2005).
[41]M. Glatthaar, N. Mingirulli, B. Zimmermann, T. Ziegler, R. Kern, M. Niggemann, A. Hinsch, and A. Gombert, Phys. Status Solidi A **202**, R125 (2005).
[42]J. Godlewski, Adv. Colloid Interface Sci. **116**, 227 (2005).
[43]R. Steim, F. R. Kogler, and C. J. Brabec, J. Mater. Chem. **20**, 2499 (2010).
[44]See supplementary material at http://dx.doi.org/10.1063/1.4767291 for a depiction of the morphologies, discussion of current edge effects, depiction of interface widths and TRIDYN-FZR simulation results.